Revision 1

Heterogeneous and retarded phase transformation of ferrihydrite on montmorillonite surface: the important role of surface interactions supplementary materials

Hongyan Wei [1,2,3], Jing Liu [4], Qingze Chen [1, 2, 3], Runliang Zhu [1, 2, 3]*, Lixia Yan [5], Yixuan Yang [1, 2, 3], Xiaoliang Liang [1, 2, 3], Jianxi Zhu [1, 2, 3], Hongping He [1, 2, 3]

1. CAS Key Laboratory of Mineralogy and Metallogeny/Guangdong provincial Key Laboratory of Mineral Physics and Materials, Guangzhou Institute of Geochemistry, Chinese Academy of Sciences (CAS), Guangzhou, 510640 China

2. CAS Center for Excellence in Deep Earth Science, Guangzhou 510640, China

3. University of Chinese Academy of Science, Beijing, 100049 China

4. State Key Laboratory of Lunar and Planetary Sciences, Macau University of Science and Technology, Taipa 999078, Macau, China

5. School of Geographical Sciences, Shanxi Normal University, Taiyuan, 030031, China

*Corresponding author. Tel: 86-020-85297603

E-mail: zhurl@gig.ac.cn

Table of content

Text S1. Materials and synthesis of the mineral heteroaggregates

Materials. The original sodium-rich Mnt (with a purity > 95%, CEC 106 mmol/100 g, and a specific surface area of 59 m^2/g) was from Inner Mongolia, China, and its chemical compositions were listed in Table S1. HCl, $Fe(NO_3)_3 \cdot 9H_2O$, NaOH, and HNO_3 were of analytical degree and were purchased from Aladdin Chemistry Co. Ltd. All chemicals were used without further treatments. All suspensions were prepared using ultrapure water (with a resistivity of 18.2 MΩ·cm).

Synthesis of the mineral heteroaggregates. To obtain Fh-Mnt, different contents of freshly prepared Fh were added to the Mnt suspension (2 wt%) under rapid stirring to obtain different mass ratios of Fh and Mnt mixtures. The suspensions containing Fh and Mnt were further titrated with freshly prepared HNO_3/NaOH to pH 6.0 ± 0.1, and then constantly stirred for 24 h at room temperature to better disperse Fh on Mnt. Subsequently, the uniform suspensions were washed three times with distilled water, followed by vacuum filtration, freeze-drying, and grinding. The resulting heteroaggregates were stored in a desiccator for the following analyses.

For synthesizing Fh/Mnt, 100 ml distilled water was added to 2 g Mnt in a 250 ml beaker, which was followed by vigorous stirring for 5 min and ultrasonic dispersion for 20 min. Then, different volumes of 1 M $Fe(NO_3)_3$ solution were added to the Mnt suspension under vigorous magnetic stirring. The amounts of Mnt and $Fe(NO_3)_3 \cdot 9H_2O$ were selected to reach a desired mass ratio of Fh to Mnt, which was calculated according to the nominal Fh molecule formula of $Fe(OH)_3$, and they were labeled as Fha/Mntb (e.g., Fh2/Mnt1 represents the mass ratio of Fh to Mnt being 2:1). The pH of the suspensions was further adjusted to 7.5 with NaOH solution. After stirring for 2 h, the suspensions were aged overnight. Similarly, the products were subject to vacuum filtration, washing, freeze-drying, and grinding, and the final samples were stored in a desiccator.

Text S2. Characterization methods

XRD: The X-ray powder diffraction (XRD) data were collected on a Bruker D8 ADVANCE X-ray diffractometer (Karlsruhe, Germany). The measurement was performed under the following conditions: Cu Kα radiation, 40 kV, 40 mA, 3-70°2θ, 0.01°2θ step and 3° 2θ min^{-1}.

FTIR: Fourier transform infrared spectroscopy (FTIR) was recorded on a PerkinElmer spectrometer. 1 mg sample powder was mixed gently with 100 mg KBr (1% sample weight) in an agate mortar and the resulting mixtures were pressed to disks. Each sample was determined in a wavenumber range of 4000 to 400 cm^{-1} in transmission mode with a resolution of 4 cm^{-1} and 64 scans. The data were analyzed using OPUS software and Origin 85. Selected regions of FTIR spectra were studied in detail through the second derivatives obtained from Origin 85. The absorption band of the spectra was shown as a negative peak in the second derivative.

SEM: scanning electron microscopy (SEM) images were acquired by a Carl Zeiss Supra 55 field emission scanning electron microscope. The samples before and after the heating treatment were mounted on conductive glue, and then fixed on the holder for morphology observation.

TEM: transmission electron microscopy (TEM) and energy diffraction spectrum (EDS) analysis were performed with an FEI Talos F200S TEM at an accelerating voltage of 200 kV. The samples were gently crushed to powder, dispersed in absolute alcohol, and sonicated before deposition on a holey copper film and dried in air. To minimize beam damage of the Fh particles, image focus and optimization were completed adjacent to aggregates of interest. High-resolution transmission electron microscopy (HRTEM) images

and selected area electron diffraction (SAED) analysis were carried out using an FEI Talos F200S high-resolution transmission electron microscope operated at 200 kV.

TG-DSC: Thermogravimetric (TG) analysis with differential scanning calorimetry (DSC) was performed on a Netzsch STA 449F3 instrument. Before analysis, the samples were dried in an oven at 50°C for 24 h. Then, the samples were heated from 30 to 1200°C at a rate of 10°C min^{-1} under a constant overflow of dry air (30 ml min^{-1}). The experiment was performed in an aluminum oxide crucible with a pierced lid.

Text S3. The procedure of calculating the particle sizes by the Scherrer equation.

The mean sizes (D) of products in different heated-treatment samples were calculated by the Scherrer equation:

$$D=K\lambda/B\cos\theta$$

Where K is a constant that is normally taken as 0.9, λ is the wavelength of X-ray (0.154056 nm), B is the full width at half maximum (FWHM) of the characteristic reflections at 2θ=33.16° (104) and 35.60° (110), and the corresponding θ is 16.58° and 17.8°, respectively. The average of these two calculated values was identified as the average particle size of Hem.

As shown in Table S3, the FWHM values used for measuring the particle size of Hem in different samples increased with rising the heating duration and the Fh content. The calculated particle sizes were included in Table S4, indicating that the particle size of Hem increased with the extended heating time. More importantly, the particle size decreased with increasing Mnt content. On the other hand, the particle sizes were also observed by the TEM, which was consistent with the calculated value.

Text S4. The procedure of heating samples by in-situ XRD.

The XRD patterns at varying temperatures were recorded using a Bruker D8 Advance with an Anton Paar Mri basic high-temperature chamber. The instrument was equipped with a Cu Kα radiation source. Samples were sprinkled on a zero-background monocrystalline silicon sheet, and then the silicon sheet was moved onto the Pt strip heater of the chamber.

For the step heating in-situ XRD characterization, the samples were recorded at 30°C and then heated from 30 to 450°C with a heating rate of 5°C s^{-1}. After the desired temperature was reached, the XRD patterns were immediately obtained in the 2θ range of 30-40° with a step size of 0.03° and 0.4 s per step.

For the real-time in-situ XRD characterization, five patterns with specified duration were recorded isothermally at 450°C (Fig S6). The evolution of the sample phase transformation could be recorded in a total time of ca. 3 h. It was obvious that the characteristic reflections of Hem in the sample of pure Fh and Fh2-Mnt1 appeared after 0.5 h (Fig. S6a-b), and Hem occurred in Fh2/Mnt1 until 3h (Fig. S6d). But for Fh1-Mnt1, there was no reflection of Hem appearing throughout the heating process (Fig. S6c). These results above stated that the Mnt can retard the phase transformation of Fh, and the inhibitory effect was correlated with the Mnt content in the heteroaggregates. Besides, Fh/Mnt shows a stronger inhibitory effect in the transformation of Fh than that in Fh-Mnt.

For the programmed heating in-situ XRD characterization, the sample was recorded at 30°C and then heated from 30 to 300°C with a heating rate of 5°C s^{-1}. After the temperature was reached at 300°C, the XRD patterns were immediately obtained in the 2θ range of 30-40° with a step size of 0.03° and of 0.4 s per step. Then the patterns were recorded at consecutive 50°C intervals from 300°C to 800°C. The single recording time was about 142 s, and the total heating time (from 30 to 800°C) of samples was ca. 0.5 h. The temperatures of occurring reflections of Hem in different samples were plotted (Fig.

S7), and the obtained results indicated that the transformation temperatures increased with increasing the Mnt content both in Fh-Mnt (Fh1-Mnt2 (700°C) > Fh1-Mnt1 (650°C) > Fh2-Mnt1 (600°C) > Fh (500°C)) and in Fh/Mnt (Fh1/Mnt2 (800°C) > Fh1/Mnt1 (700°C) > Fh2/Mnt1 (650°C) > Fh (500°C)). In addition, the temperatures of the Hem reflections occurring in Fh/Mnt were higher than the counterpart Fh-Mnt. Fh2/Mnt1 (650°C) > Fh2-Mnt1 (600°C). As a result, Mnt retarded the transformation of Fh and the inhibitory effect was stronger in the Fh/Mnt than that in Fh-Mnt.

Table S1. The chemical compositions of Mnt

Composition	Content (%)	Composition	Content (%)	Composition	Content (%)
Al_2O_3	15.94	SiO_2	59.38	SO_3	0.01
CaO	2.93	Na_2O	3.18	MnO	0.04
Fe_2O_3	4.82	TiO_2	0.31	BaO	0.01
K_2O	0.21	SrO	0.02	Cr_2O_3	<0.01
MgO	4.95	P_2O_5	0.03	LOI	8.03

Table S2. The assignment of the corresponding FTIR absorption bands

Position (cm^{-1})	Assignment	Position(cm^{-1})	Assignment
3623	Structural Al-OH stretching	779-801	Si-O bending (Quartz)
3397-3426	Stretching of adsorbed H_2O	594	Fe-O stretching (Fh)
1627-1638	Bending of adsorbed H_2O	472	Fe-O stretching (Fh)
1384	Stretching of NO_3^-	542	Fe-O stretching (Hem)
960-1200	Si-O stretching	468	Fe-O stretching (Hem)
913-915	Al-Al-OH bending	519	Al-O-Si deformation
837	Al-Mg-OH deformation	466	Si-O-Si deformation

Table S3. The FWHM used for measuring the particle size of Hem in different systems. The FWHM values decrease with raising the heating time and the content of Fh

Sample name	FWHM (104)	FWHM (110)
Fh-400-1	0.564	0.585
Fh-400-2	0.433	0.393
Fh-400-4	0.412	0.331
Fh2-Mt1-400-4	0.458	0.414
Fh1-Mt1-400-4	0.654	0.596

Table S4. The mean size of Hem particles measured by the Scherrer equation and observed by TEM.

Sample name	Scherrer equation (nm)	TEM observation (nm)
Fh-400-1	14.5	*
Fh-400-2	20.2	*
Fh-400-4	22.7	27.4
Fh2-Mt1-400-4	19.1	17.5
Fh1-Mt1-400-4	13.3	7.5

*The sample did not observe in the TEM.

Figure S1. Morphology of original Fh and Mnt. **(a)** TEM image of Fh nanoparticles. **(b)** SEM image of Mnt, and the pores in Mnt are highlighted by the yellow arrows.

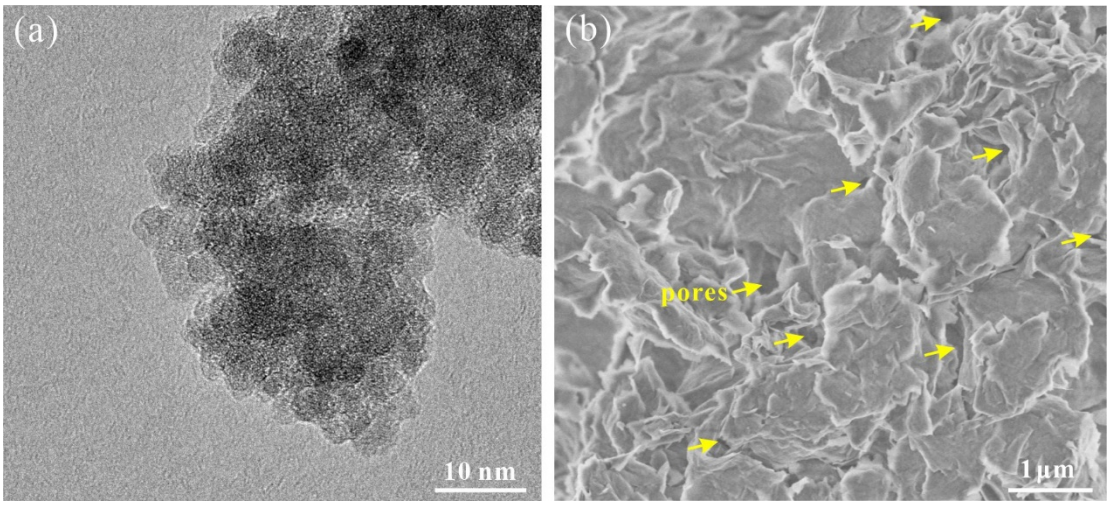

Figure S2. Distribution of different elements in Fh2-Mnt1. **(a)** TEM image of Fh2-Mnt1. EDS mapping of **(b)** Fe, **(c)** Si, and **(d)** Al, indicating that the distribution of Fh in Fh-Mnt is uneven. **(e)** The relative content of Al, Si, and Fe in the selected areas from a, and the red dash line marks the theoretical content of Fe in the sample.

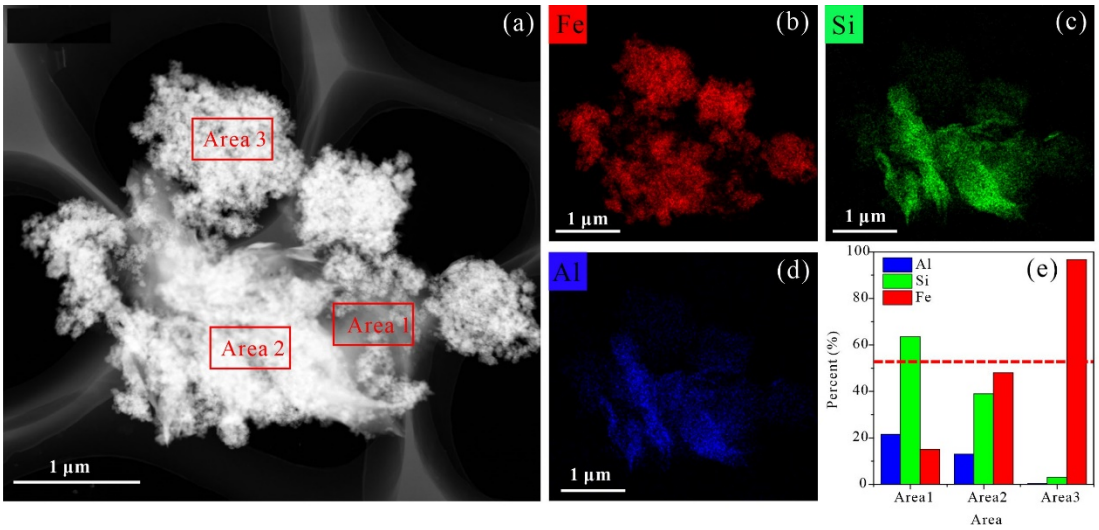

Figure S3. Distribution of different elements in Fh2/Mnt1. **(a)** TEM image of Fh2/Mnt1. EDS mapping of **(b)** Fe, **(c)** Si, and **(d)** Al. **(e)** The relative content of Al, Si, and Fe in the selected areas from a, and the red dash line represents the theoretical content of Fe in the sample.

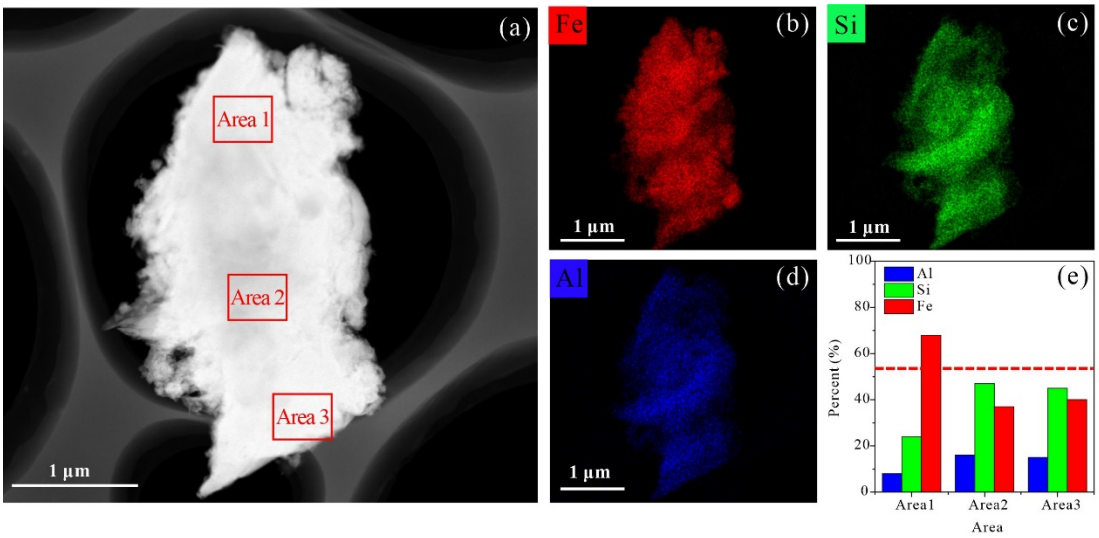

Figure S4. (a) FTIR spectra of Mnt, Fh2-Mnt1, Fh2/Mnt1, and Fh before heating. **(b)** The second derivatives curves in the range of 750-1300 cm^{-1} in the box of a.

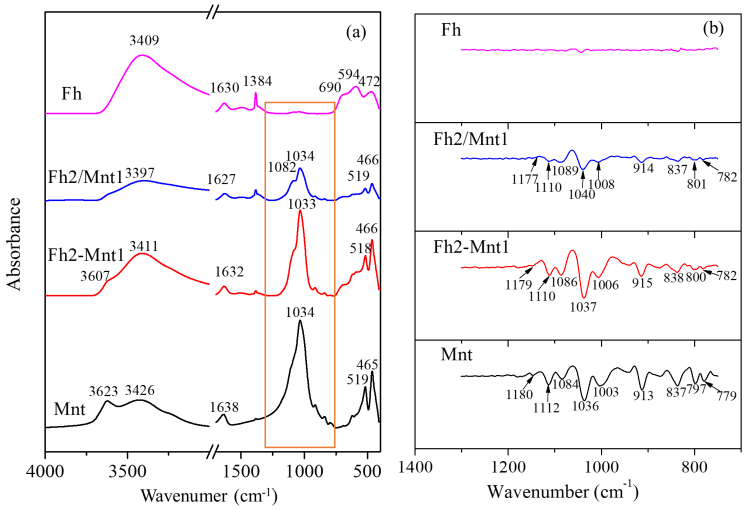

Figure S5. XRD patterns of different samples heating at different temperatures and times. **(a)** XRD patterns of Fh and the thermally treated products at different temperatures and durations. **(b)** XRD patterns of Mnt after heating at different temperatures and durations.

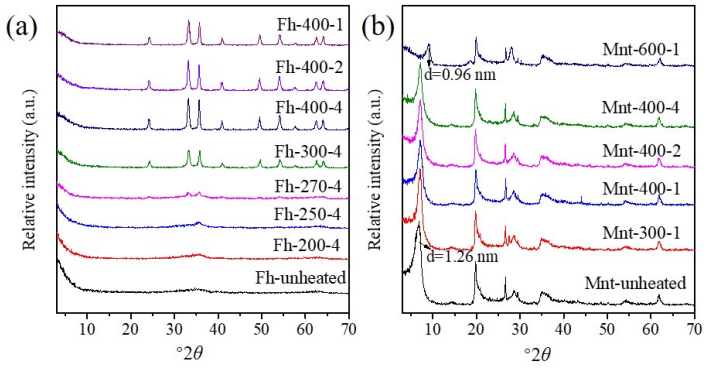

Figure S6. The in-situ XRD patterns of different samples heating at 450**°C** at different intervals. **(a)** Fh, **(b)** Fh2-Mnt1, **(c)** Fh1-Mnt1, and **(d)** Fh2/Mnt1. The results shows that the inhibitory effect of Mnt on the transformation of Fh.

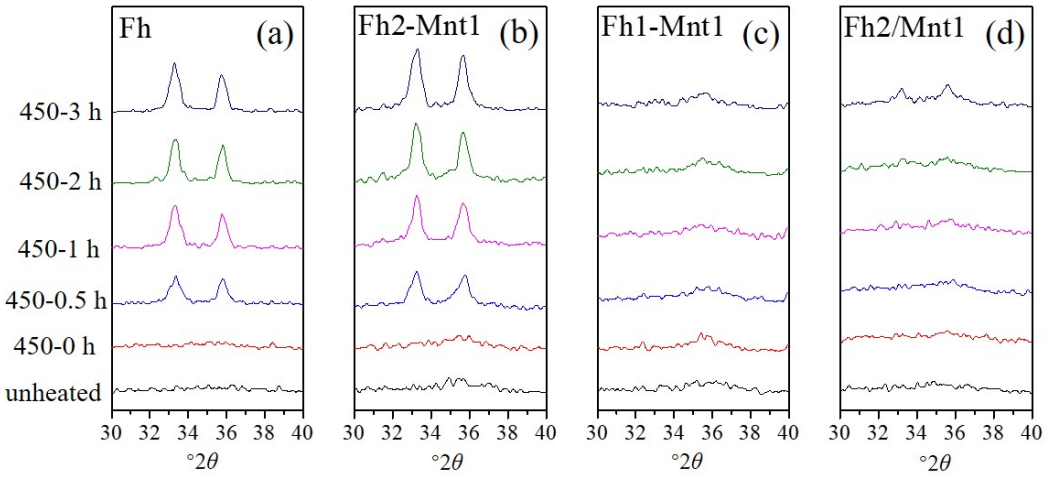

Figure S7. In-situ XRD patterns of different samples recording from 30°C to 800°C. **(a)** Fh, **(b)** Fh2-Mnt1, **(c)** Fh1-Mnt1, **(d)** Fh1-Mnt2, **(e)** Fh2/Mnt1, **(f)** Fh1/Mnt1, **(g)** Fh1/Mnt2. **(h)** The temperatures of the reflections of Hem occurring in different samples, and 2Fh:1Mnt represents the mass ratio of Fh and Mnt is 2:1.

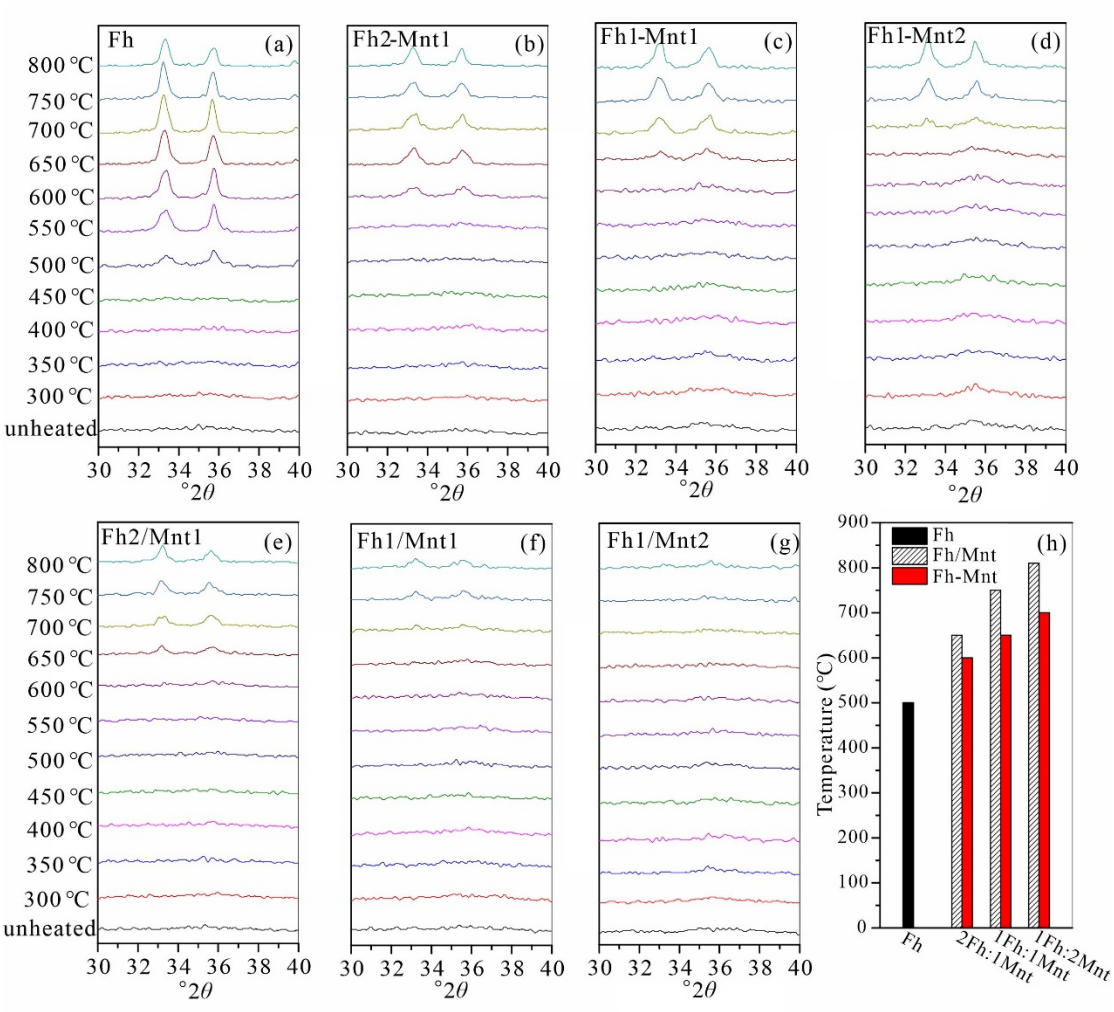

Figure S8. TEM images of Fh2-Mnt1-600-1. **(a)** TEM image. **(b and c)** EDS mapping of a. **(d and e)** the SAED of the marked area "d" and "e" in Fig. a. **(f)** HRTEM image of Hem with lattice planes of (110) and (220). The disappearance of diffraction rings of Fh shows that the transformation of Fh was nearly complete.